Selection of the optimum magnet design for the International Linear Collider positron source helical undulator

D. J. Scott,[*,†,‡] S. Appleton,[‡] J. A. Clarke,[‡] O. B. Malyshev,[‡] B. J. A. Shepherd,[‡] and B. Todd
CCLRC Daresbury Laboratory, Daresbury, Warrington, Cheshire WA4 4AD, United Kingdom

D. E. Baynham, T. Bradshaw, A. Brummitt, S. Carr, Y. Ivanyushenkov, and J. Rochford
CCLRC Rutherford Appleton Laboratory, Chilton, Didcot, Oxfordshire OX11 0QX, United Kingdom

I. R. Bailey,[‡] P. Cooke, J. B. Dainton,[‡] and L. I. Malysheva[‡]
Department of Physics, University of Liverpool, Oxford St., Liverpool, L69 7ZE, United Kingdom

D. P. Barber[‡]
DESY-Hamburg, Notkestraße 85, 22607 Hamburg, Germany

G. A. Moortgat-Pick[‡]
Institute of Particle Physics Phenomenology, University of Durham, Durham DH1 3LE, United Kingdom, and CERN, CH-1211 Genève 23, Switzerland
(Received 24 August 2006; published 30 March 2007)

A comparison of possible undulator designs for the International Linear Collider positron source has resulted in a superconducting bifilar wire design being selected. After a comprehensive paper study and fabrication of the two preeminent designs, the superconducting undulator was chosen instead of the permanent magnet alternative. This was because of its superior performance in terms of magnetic field strength and quality, operational flexibility, risk of radiation damage, ease in achieving the required vacuum, and cost. The superconducting undulator design will now be developed into a complete system design for the full 200 m long magnet that is required.

DOI: 10.1103/PhysRevSTAB.10.032401 PACS numbers: 07.85.Qe, 85.70.Ay

I. INTRODUCTION

The baseline design for the International Linear Collider (ILC) positron source is based on multi-MeV photons pair producing in a metallic target [1]. The photons are created by the main electron beam passing through a helical undulator. A source of this kind was first described in 1979 [2] and was adopted for the TESLA collider design as an upgrade to polarized positron production [3].

For the ILC design, the high energy ($\sim$ 150 GeV) electron beam from the electron linac passes through a helical undulator generating $\sim$10 MeV synchrotron radiation at the first harmonic cutoff. (In the TESLA design, for which this work initially started, the undulator was at the 250 GeV point in the linac and was optimized to produce $\sim$20 MeV photons at the first harmonic cutoff.) If the circularly polarized (CP) radiation from the helical undulator is selected, for example, by photon collimation, then this polarization is transferred to the electron-positron pairs and a polarized positron beam can be generated. The higher the CP rate of the photon beam, then the higher the polarization of the resultant positron beam. Theoretical studies and computer analyses have shown that a polarized positron beam could greatly enhance the physics reach of the ILC [4].

A schematic of the current ILC layout with main positron source components is shown in Fig. 1. While exact values for parameters, such as the degree of circular polarization and undulator field integrals, are not yet fixed, a nominal set of parameters has been chosen in order to evaluate the possible alternative solutions. Table I gives the baseline parameters for the ILC [1]. This is because simulation of the source is a multidimensional problem with many cross-talking parameters, e.g., the target material and thickness, positron capture efficiency, and degree of photon collimation. However, increasing the length of the undulator will solve most problems. For example, if the degree of circular polarization is not high enough then more photon collimation will be required; therefore an increased length of active undulator will be required to maintain the positron intensity. The length of undulator required is $\sim$100 m for an unpolarized positron source and is anticipated to be $\sim$200 m for a polarized positron source, although these numbers depend upon many assumptions that have yet to be confirmed, such as the performance of realistic undulators.

Recently a proof of principle experiment, Experiment-166 [5], demonstrating polarized positron production using

[*]Electronic address: d.j.scott@dl.ac.uk
[†]Also at Department of Physics, University of Liverpool, Oxford St., Liverpool, L69 7ZE, UK.
[‡]Also at The Cockcroft Institute, Daresbury Laboratory, Warrington, Cheshire, WA4 4AD, UK.

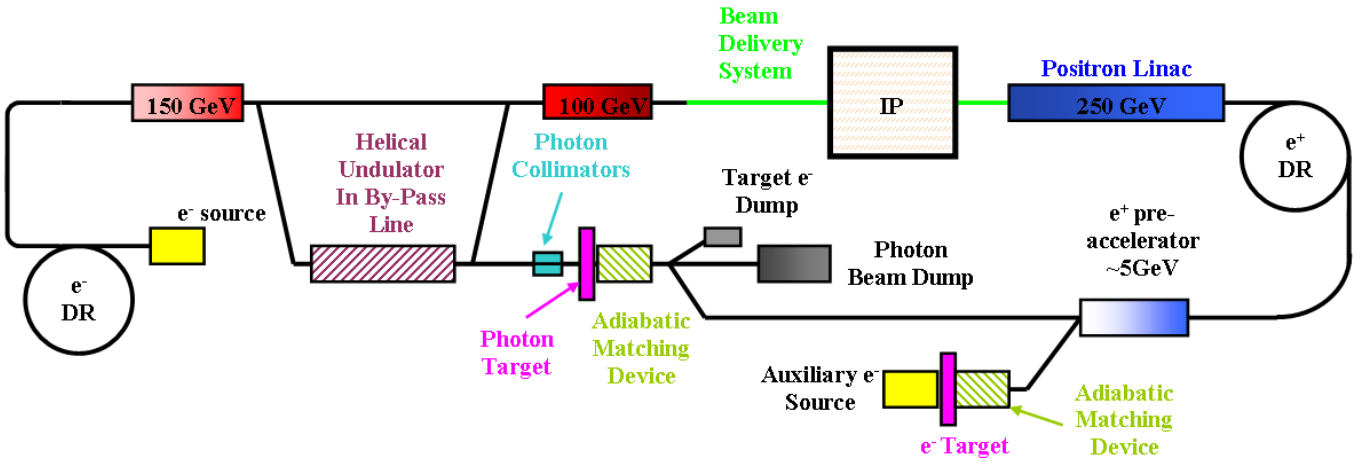

FIG. 1. (Color) ILC schematic layout with main positron source components. The undulator is placed at the 150 GeV point of the main linac in a by-pass line so that the axis of the generated photon beam is separate from the axis of the main electron beam. Photons incident on the target produce electron-positron pairs via pair production. The positrons are captured and accelerated in the adiabatic matching device and then accelerated to 5 GeV in the preaccelerator. They are then transported to the positron damping ring and then on to the main positron linac. DR stands for the damping rings and the auxiliary electron source represents a low intensity conventional positron source to be used when the undulator source is not functioning.

a helical undulator has been completed at the Stanford Linear Accelerator Center. Initial results indicate polarized positrons were created and detected [6].

The aim of this work is to explore possible undulator designs and assess their suitability. The issues that are of obvious concern are the ease of fabrication of the undulator, achieving a suitable magnetic field strength and quality, and the operational reliability and flexibility of the device. The other important issue is achieving the vacuum specification of 10^{-8} mbar (CO equivalent), which is required to keep the emittance dilution due to the fast ion instability at an acceptable level. This is challenging due to the narrow-gap vessel that needs to be used to achieve the high magnetic fields needed in the device.

TABLE I. Nominal positron source parameters.

Parameter	Value	Units
Positrons per bunch	2×10^{10}	
Bunches per pulse	2820	
Pulse repetition rate	5	Hz
e^- energy	150	GeV
Nominal undulator period	10	mm
Nominal undulator K	1	
Undulator type	helical	
Nominal undulator length (unpolarized source)	~100	m
Photon energy (1st harmonic cutoff)	~10	MeV
Max photon beam power (unpolarized source)	~150	kW
Nominal target material	Ti-6%Al-4%V	
Nominal target thickness	0.4	Radiation lengths
Max target power absorption	<15	kW
Nominal vacuum	10^{-8}	mbar
Positron polarization (upgrade)	60	%
Nominal undulator length for polarized positrons	~200	m

II. UNDULATOR DESIGN

In the ILC baseline design a helical undulator with a period, $\lambda_u = 10$ mm, and an undulator K parameter of 1 is assumed. Where K is a dimensionless parameter that is defined as

$$K = \frac{Be\lambda_u}{m_e c 2\pi},$$

where B is the peak on-axis magnetic field, m_e is the electron mass, e the electron charge, and c the speed of light. The maximum angle of deflection experienced by an electron in an undulator is given by the K parameter divided by the relativistic γ of the electron.

A helical undulator with these parameters has not been experimentally demonstrated yet. A paper study into various helical undulator designs based on permanent magnet (PM) and superconducting (SC) undulators was carried out. Model test pieces of the most promising designs were constructed to assess the ease of fabrication and to confirm the magnetic field strength and quality. For all the designs, it was assumed that the minimum aperture could be ~4 mm. This number was set by the TESLA design team as it was equivalent to the minimum aperture that could be tolerated by the TESLA design. For all the following, the z direction shall be the longitudinal axis,

the x direction the vertical axis and the y direction the horizontal axis.

A. Pure permanent magnet designs

Synchrotron light sources have used planar arrays to produce on-axis helical field distributions for over 20 years. For light sources, the planar configuration suits the large horizontal to vertical beam-size ratio. Planar helical undulators offer a number of advantages as they are a proven technology with well understood engineering solutions. They also allow easy access to the vacuum vessel which is required if a nonevaporable getter (NEG) coated vessel is used. Three different planar helical PM undulators were considered, the multimode undulator [7,8], the APPLE-II [9], and a new APPLE design, the APPLE-III [10].

A helical field can also be created by using an array of stacked dipole rings in which the dipole field is rotated from ring to ring. Each period of the undulator is divided up into rings. Each ring is comprised of trapezoidal PM blocks that produce an on-axis transverse dipole field by rotation of their magnetization vectors by 4π radians around the ring [11] (shown in Fig. 2 for 8 magnet blocks in a ring). The dipole field of each ring is rotated with respect to the preceding one so that over one period the total rotation of the on-axis dipole field is 2π radians [12].

The different undulator designs were modeled in the magnetostatics code RADIA [13] to find the peak on-axis magnetic field, B. In all cases the minimum magnetic gap, or aperture in the ring undulator, was chosen to be 4 mm. The planar undulators were modeled in circularly polarizing mode. Figure 3 shows λ_u vs B for each model as well as the required period and field to produce 20 MeV photons with a 250 GeV beam and 10 MeV photons with a 150 GeV beam. The PM material used was NdFeB with a remanent magnetization of 1.3 T. As expected, the PM ring undulator out-performs the planar helical undulators as there is magnetic material surrounding the vacuum chamber driving more flux into the aperture.

The multimode undulator has 6 arrays compared to the APPLE-II and APPLE-III's four arrays which means it can produce a high on-axis field in circularly polarizing mode. The APPLE-III design has notches cut into the magnet blocks so they are closer to the magnetic axis giving a higher field on-axis than the APPLE-II design. To minimize the total length of undulator required, the 14 mm period PM ring undulator was chosen. (N.B. some of the parameter choices made in this study reflect the fact that this work was initially started for the TESLA project, and may not be fully optimized for the ILC baseline.)

To achieve the specified vacuum in the vessel of 10^{-8} mbar (CO equivalent), the vacuum vessel would need to be coated with a NEG coating. NEG coating requires activation by high temperature bakeout and so access to the vessel, with no surrounding magnetic material, would be required. Therefore the undulator was designed to be split into two halves, since the temperature required to activate the NEG would otherwise demagnetize the PM blocks. To keep the design regular (i.e. smooth along the faces of each half), the number of blocks per ring must be an even number and must be a multiple of the number of rings per period.

Another issue that was considered was the magnetic force between the arrays. The force between the two undulator halves can be considerable and depends on the detailed configuration of the magnet blocks. Figure 4 shows the magnet forces between the arrays for ten periods

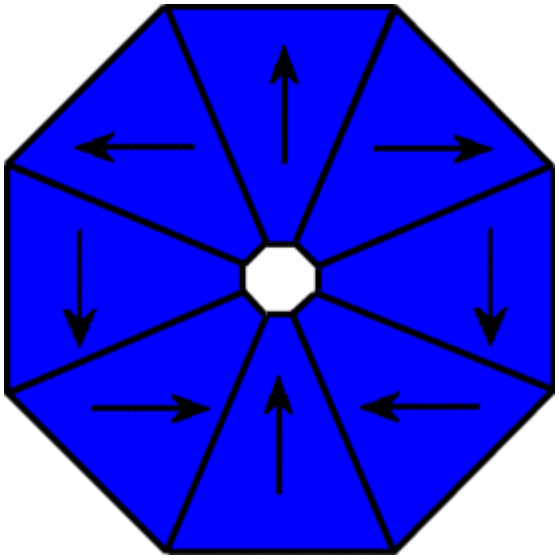

FIG. 2. (Color) Schematic showing the magnetization vectors of a dipole ring comprised of 8 magnet blocks. For 8 blocks in a ring, the magnetization vector must be rotated by 90° from block to block to produce a dipole field on-axis.

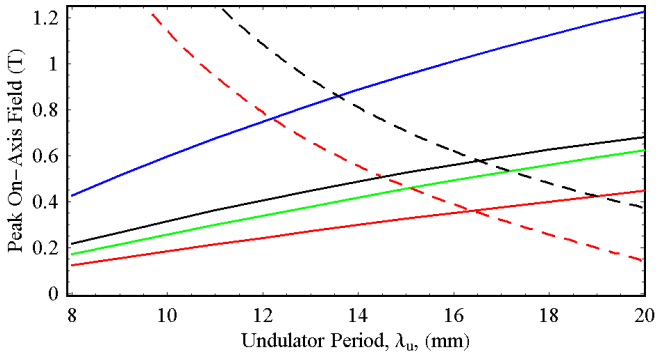

FIG. 3. (Color) Computer modeled peak on-axis magnetic field for APPLE-II (solid, red), APPLE-III (green), multimode (solid, black) undulators in circular polarizing mode and for the PM ring undulator (blue) vs undulator period length. The field/period length required to produce 10 MeV photons with 150 GeV electron beam (dashed, red) and 20 MeV photons with a 250 GeV beam (dashed, black) at the first harmonic is also shown.

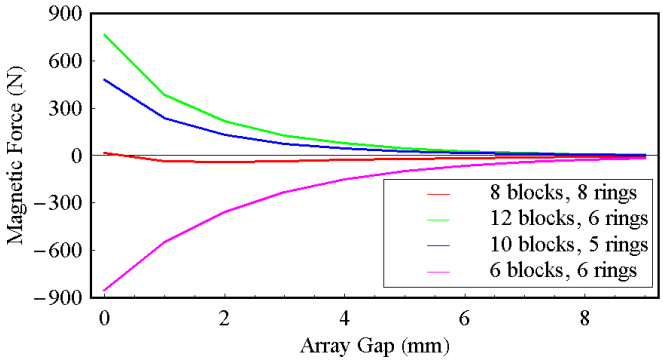

FIG. 4. (Color) Magnetic forces between the arrays for 10 periods of different PM ring undulator configurations. The legend gives the number of blocks making a single ring and the number of rings making a period.

of a 14 mm period device as a function of the array gap. The first number in the legend refers to the number of PM blocks making a ring and the second number gives the number of rings in a period. It can be seen that the force between the two halves can either be repulsive or attractive, depending upon the configuration. A typical length for a PM undulator would be 5 m and so the forces between the arrays could be as high as 30 kN at zero magnetic gap. This would make the engineering of the support girders and gap control mechanism quite demanding. To make the supporting structure as simple as possible, an 8 blocks per ring/8 rings per period configuration was chosen as this minimizes the forces between each array at all gaps.

A ten period model was chosen to be made to allow for measurement of the magnetic field away from any end effects. Wedges of PM material were made up of identically shaped pieces with a rotated axis of magnetization (left side of Fig. 5). Four wedges were then glued into aluminum holders to make half of a ring (center of Fig. 5). The aluminum holders were then aligned and fastened to top and bottom array base plates, which could then be fitted together in the final assembly (right side of Fig. 5). A photograph of the completed undulator is shown in Fig. 6.

The tolerance on the deviation of the magnetization vector direction from the ideal direction was specified to be $\pm 3°$, after thermal stabilization, compared to $\pm 1.5°$ commonly used in undulators for synchrotron light sources. This is because it would have been difficult to do much better due to the block geometry (without excessive costs). It was also decided that no block sorting algorithm would be used. Typically undulator magnet blocks are sorted (i.e. their exact orientation and position in the undulator array is specified) to minimize a weighted objective function comprised of field integrals, phase errors, and other relevant parameters. This process is time consuming and, for undulators in excess of 100 m long, this procedure is impractical. For this design there would be nearly a half million magnet blocks to sort for 100 m of undulator. This approach has also been proposed for the European x-ray laser project undulators that are of a similar scale [14].

B. Superconducting magnet design

This design is based on two helical superconducting windings wound around a vacuum vessel. The windings are spatially shifted a half period in the longitudinal direction and current is passed through each winding in opposite directions. With current flowing, the on-axis longitudinal magnetic field cancels leaving only a helical transverse field. A number of devices have been made in this manner [15,16].

Extensive magnetic modeling was carried out in order to select the winding geometry of the undulator [17]. The

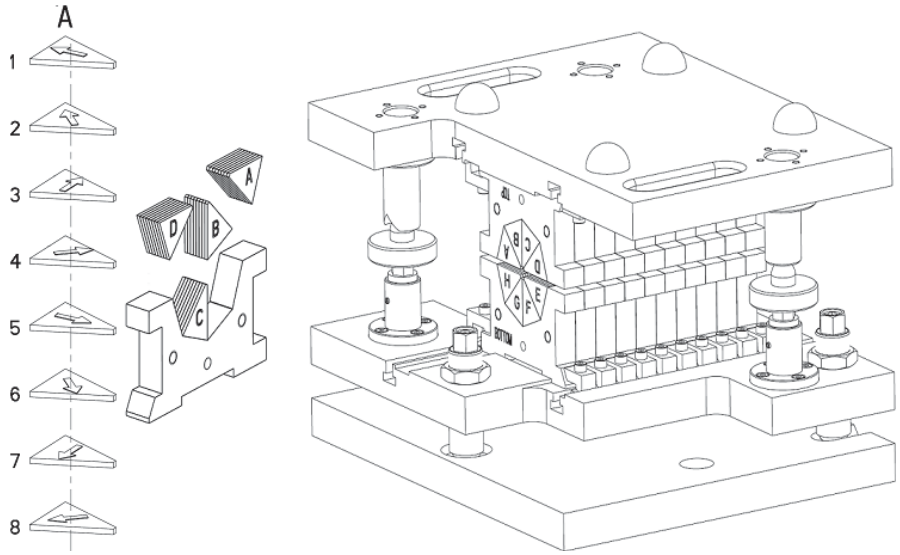

FIG. 5. Assembly drawing of PM ring undulator.

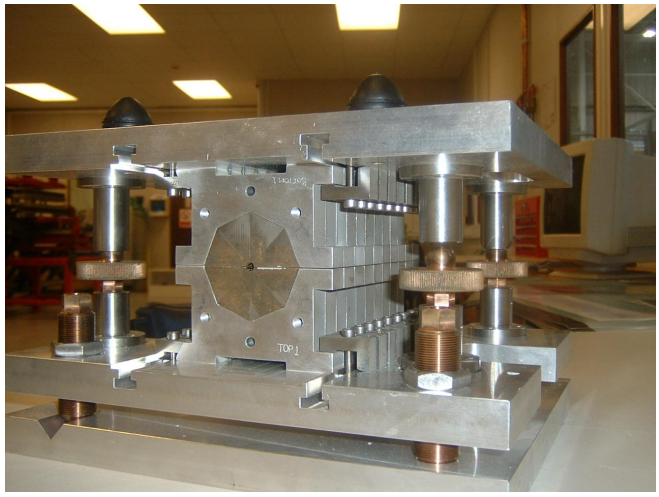

FIG. 6. (Color) Photograph of completed PM ring undulator assembly, with ten 14 mm periods.

software packages OPERA 2D and 3D from Vector Fields Ltd. [18] were used for the modeling studies. The results of the magnetic modeling indicate that: (i) A winding with a flat shape (with the minimal radial height to width ratio) creates maximal field on-axis for a given current density. However, taking into consideration the peak field in the conductor, a square shape was found to be optimal. (ii) The peak field in the conductor is about twice the field on the undulator axis. The highest field in the conductor is always in the internal layers of the winding (Fig. 7).

Undulator conductor load lines, shown in Fig. 8, were calculated and are expressed as a percentage of the short sample critical current, for a winding geometry of 8 layers

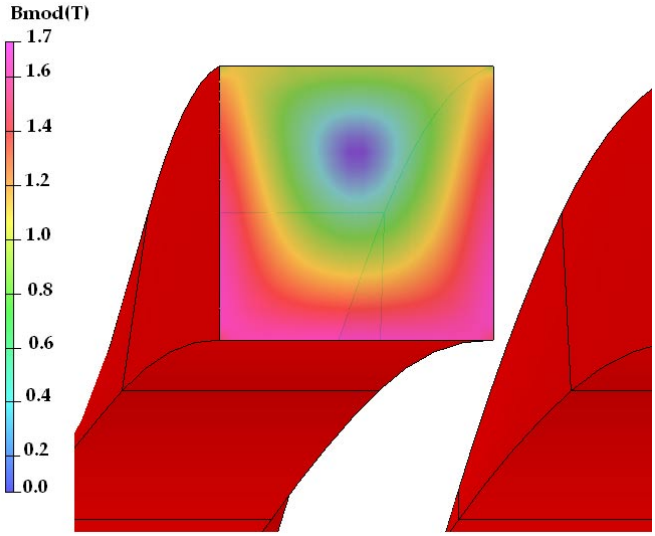

FIG. 7. (Color) Calculated magnetic flux density (Bmod) through a cross section of the conductor windings for a current density of 1000 A mm^{-2}. The highest flux is in pink near the axis of the magnet and is 1.75 T. The lowest flux is in blue near the center of the winding and is 77 mT.

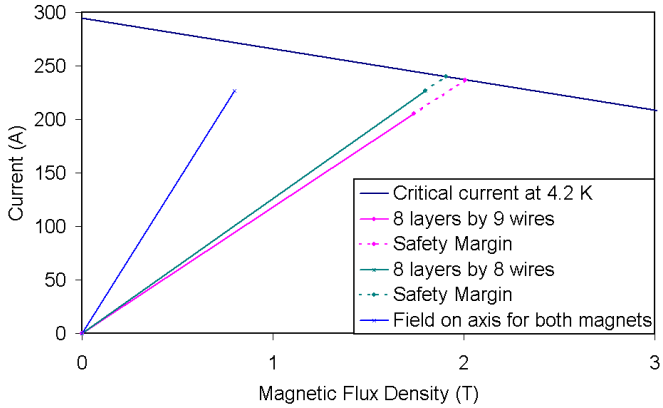

FIG. 8. (Color) Undulator conductor load lines, critical current at 4.2 K, and the field achieved on-axis.

with 8 wires in a layer and for 8 layers with 9 wires in a layer. The 9×8 winding operates at 86% of the critical conductor giving a safety margin of 14%. The 8×8 winding operates at 94% of the critical current and the safety margin is 6%. The prototype uses an 8×8 winding geometry as it was not possible to fit a 9-wire ribbon into the rectangular groove of the first former. Future former designs will use a trapezoidal geometry to accommodate a 9-wire ribbon. A period of 14 mm was chosen as the computer model predicted the required field could be achieved. This also allowed for a fair comparison with the PM magnet.

The undulator was wound with superconducting wire, VACRYFLUX 5001 type F54 [19], onto an aluminum former 20 periods long. The internal bore of the former was 4 mm and the winding bore was 6 mm. Preliminary work indicated that winding the undulator with a wire ribbon rather than a single wire could significantly reduce technical difficulties encountered at the ends of the multi-

FIG. 9. (Color) Photograph of undulator winding showing the return pegs to allow for continuous winding.

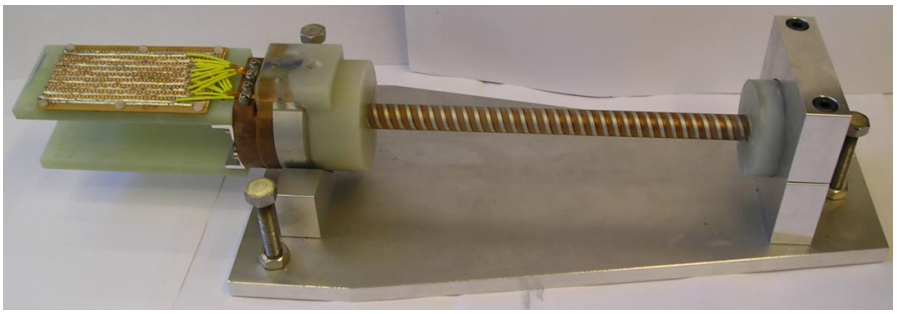

FIG. 10. (Color) Photograph of the completed SC undulator before field measurement, with 20 14 mm periods.

wire winding. A similar approach is implemented at CERN for the winding of Large Hadron Collider corrector magnets [20].

Eight 0.44 mm wires were bonded in a flat ribbon with a width of approximately 4 mm and a thickness of 0.5 mm. The ribbon was then wound into a spiral groove in the former. To achieve a continuous winding of two helices in one operation, two sets of pegs were used at the ends of the undulator for the return of the ribbon into the adjacent helical groove (Fig. 9).

After winding, the undulator coil was vacuum impregnated with epoxy resin and the wires in the ribbon were interconnected at the terminal block to form the series winding. As a result, the undulator winding forms a multilayer, continuous, double helical, winding with two leads for connection to a power supply. The final view of the undulator before installation into the cold test rig is shown in Fig. 10.

III. MAGNETIC MEASUREMENTS

After fabrication of the two models, magnetic field measurements were taken and these are detailed below.

A. PM ring undulator measurements

The direction and magnitude of the magnetization vector for each individual block were measured before assembly and their position in the assembly recorded. From this data the expected magnetic field was calculated with RADIA. The on-axis field of the assembled magnet was measured using a conventional Hall probe measuring bench. The probe was mounted on a stiff carbon fiber shaft and aligned to the axis of the bench. The ratio of planar Hall effect coefficient to normal Hall effect coefficient for the Hall probe is a maximum of 8×10^{-4}. This means that the maximum magnetic field error will be $\sim$0.3 mT when measuring a zero field perpendicular to the Hall probe. Figure 11 shows the measured field, expected measurements (from the individual block data), and ideal field in the two transverse directions, x and y, respectively. First and second field integrals in the transverse directions ($I_{x,y}$, $J_{x,y}$), undulator K parameters, and the mean on-axis peak field neglecting the ends are given in Table II. For a 150 GeV electron beam the final angles at the end of the undulator are 3.9 and 6.4 nrad in the x and the y direction, respectively. The final displacements off axis are -460 and -652 nm in the x and y directions, respectively. The trajectory is shown in Fig. 12.

The computer modeled field is less than the ideal field due to the magnetization errors of the individual magnet blocks. As can be seen from the comparison of the ideal and computer modeled results, the magnetization vector errors can result in a decrease in the peak field strength of $\sim$0.15 T. As the ILC polarized positron source requires an undulator $\sim$200 m in length, it is important to minimize the costs of individual magnets where possible. Relaxed specifications requiring lower production costs were therefore chosen for the permanent magnets in order to ascertain whether the required field could be realized economically. The tolerance on the deviation of the magnetization vector direction from the ideal direction was specified to be $\pm 3°$, after thermal stabilization, compared to $\pm 1.5°$ commonly used in undulators for synchrotron light sources. Therefore

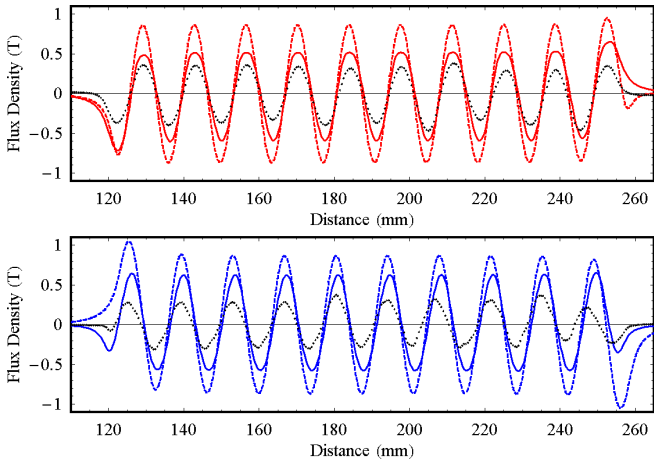

FIG. 11. (Color) Ideal (dashed) computer model based on actual block measurements (solid) and measured (points) on-axis magnetic flux density in the x direction (top) and y direction (bottom) for the PM ring undulator.

TABLE II. PM and SC undulator field measurement data.

Parameter	Unit	PM undulator	SC undulator
I_x, I_y	T m	-1.9×10^{-6}, -3.2×10^{-6}	6.8×10^{-9}, 3.8×10^{-7}
J_x, J_y	T m^2	-2.3×10^{-4}, -3.3×10^{-4}	1.5×10^{-5}, 2.7×10^{-5}
K_x, K_y		0.39, 0.47	1.06, 1.06
On-axis peak field	T	0.30, 0.36	0.81, 0.81

the modeling indicates that high quality magnet blocks should be used if the ideal peak field is to be obtained.

The measured field is less than was expected from the computer model: this could be due to a number of effects. Although every effort was made to ensure each block was measured accurately and aligned correctly in the assembly, mistakes may have been made. This is not possible to check as the blocks are now bonded together. Also, the strong demagnetizing field that blocks experience when compiling the wedges, assembling the wedges into the holders, and then bringing the two arrays together has reduced their remanent field strength and working point. As an example of the demagnetizing fields experienced when assembling the magnet, the maximum reverse field in a single block was calculated as the nearby magnet blocks were assembled. The assembly of the wedge and the two adjacent wedges is shown in Fig. 13. Using the numbers in Fig. 5 to represent the different orientations of the block magnetization vector, the first block in Fig. 13 is of type 5, the second (red) block is of type 6, the third block is of type 7, etc.

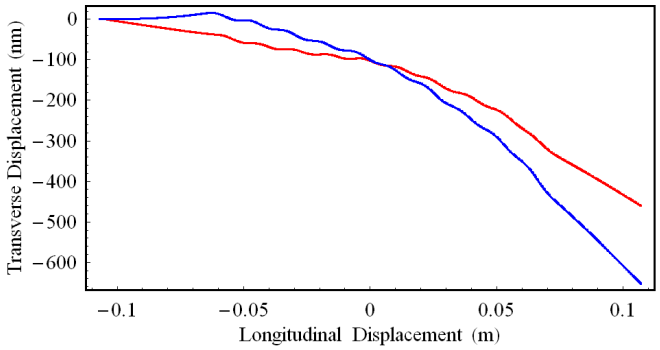

FIG. 12. (Color) Calculated trajectory in the transverse x (red) and y (blue) directions for the PPM undulator.

The peak reverse fields in the red block (Fig. 13) as it is slid into place and as the other blocks are slid over it to form a complete wedge, and then as the two adjacent wedges are also slid into place, are shown in Fig. 14. A peak reverse field of 1080 kA m^{-1} is experienced when blocks 7 and 8 are slid into position. After the other blocks and adjacent wedges are added the peak reverse field is only 800 kA m^{-1} in the red block. The specification of the coercivity was 950 kA m^{-1} which is adequate for the peak reverse fields in the blocks in their final position, but is not sufficient given the reverse fields experienced by the magnet blocks in assembling the wedges and periods. The effect of a reverse field of this strength is to irreversibly reduce their remanent field strength, and hence the total on-axis field provided by the undulator. Blocks with a lower remanent field but higher coercivity should have been chosen to negate any demagnetizing effects.

To accurately retest the demagnetization of each of the blocks would require the magnet to be disassembled and the magnetic field strength and direction of the individual blocks remeasured. However, this is impractical due to the strength of the bonding and the low intrinsic strength of the individual magnet blocks, also further demagnetization would probably occur in disassembly. Unfortunately, as

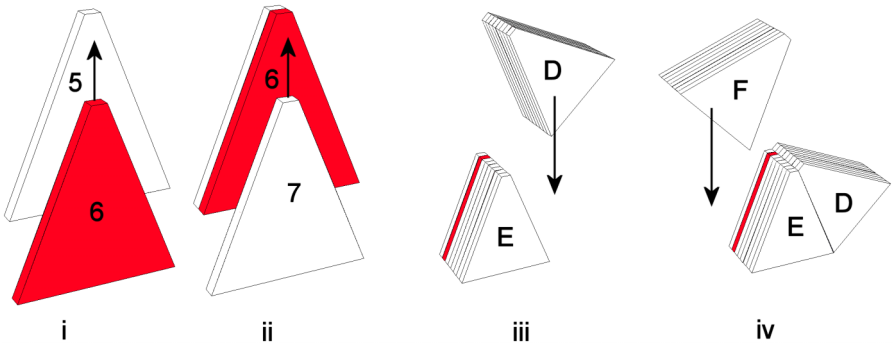

FIG. 13. (Color) The maximum reverse field in the red block was calculated as it is assembled into a wedge (i), as the rest of the blocks in the wedge are added (not all blocks are shown) (ii), and as the two adjacent wedges are added (iii and iv). The block numbers and wedge letters are determined from Fig. 5.

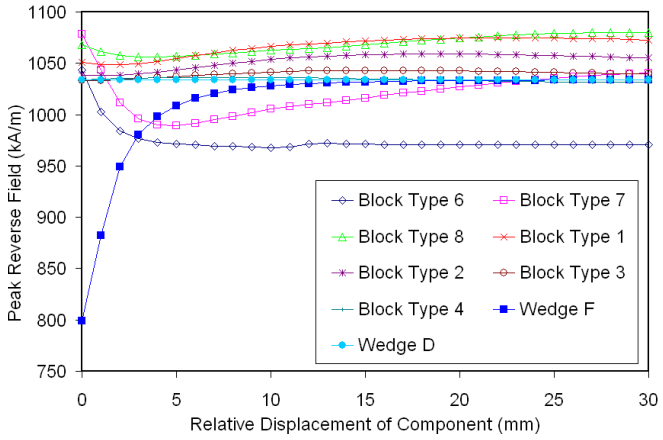

FIG. 14. (Color) The peak demagnetizing field inside the sample block as other blocks and wedges (shown in Fig. 13) are slid into position.

no block sorting was to be performed, no spare blocks were purchased on which further tests could be performed.

B. SC undulator measurements

The undulator was mounted vertically in a liquid helium bath. The level of liquid helium in the cryostat was monitored with discrete level sensors to ensure that liquid helium covered both the undulator coil and the superconducting current leads. The temperature of the undulator was monitored during cool-down and operation. Voltage taps were used to measure the resistive voltage across the undulator coil with a nanovoltmeter when the undulator was powered. In the cold test, the undulator reached the maximum current of the power supply at 225 A without quenching. The voltage across the complete undulator coil was at the level of 10^{-6} V. This indicates that the wire interconnections have a total resistance $<10^{-8}\ \Omega$. The undulator field profile, measured at a current of 220 A, is shown in Fig. 15 and has the expected peak field. It was measured using a Hall probe similar to the pure PM undulator measurements that was calibrated for 4 K operation by the manufacturers. The first and second field integrals, K parameters and mean on-axis peak field are given in Table II. For a 150 GeV electron beam the final angles at the end of the undulator are 14 and 762 prad in the

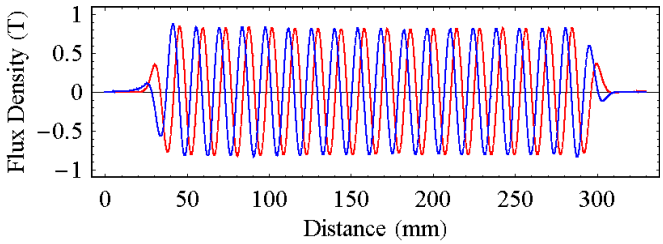

FIG. 15. (Color) Measured on-axis magnetic field in both transverse directions for the SC undulator.

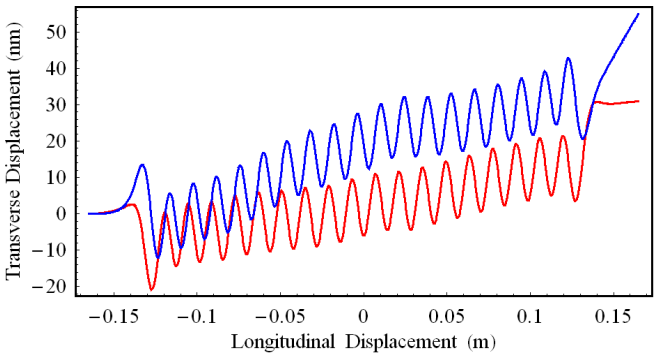

FIG. 16. (Color) Calculated trajectory in the transverse x (red) and y (blue) directions for the SC undulator.

x and the y direction, respectively. The final displacements off axis are 30.9 and 54.9 nm in the x and y directions, respectively. (Although these numbers sound incredibly small it must remembered that the electron beam is extremely rigid and the total length of undulator is only ~0.3 m.) The trajectory is shown in Fig. 16.

IV. PHOTON FLUX AND POLARIZATION

From the measured magnetic field of the undulators, the radiation spectrum and polarization can be calculated. This was done using the numeric code SPECTRA [21] and is shown in Fig. 17 for an ILC beam with parameters as given in Table III for the two different models. Two different beam energies have been considered to show the difference between the TESLA and ILC designs. Table IV gives the peak flux and circular polarization rate.

Because of interference effects, characteristic of all undulator radiation, there will be some spectral broadening in the photon spectrum due to the finite length of the undulators. The FWHM of the ten period PM undulator device is approximately a factor of 2 larger than the FWHM of the 20 period superconducting device for each harmonic peak, as can be seen in the widths of the first harmonics in Fig. 17. For the real ILC undulator, this would not be a significant factor as both devices would have many thousands of periods. The difference between the total number of photons for the two undulators is explained by the differing K parameters. The total photon flux scales linearly with the undulator length and determines the maximum positron intensity in the ILC positron source. As the PM undulator produces less photons per unit length, it would consequently have to be longer to produce the same positron intensity as the SC undulator. The circular polarization rates are between 0.78 and 0.93 and although there is no specification for the ILC it is assumed that these rates, being close to the ideal value of 1, are acceptable. The polarization rates for the SC undulator results are higher than those for the PM undulator because the magnetic field quality in the SC undulator is better.

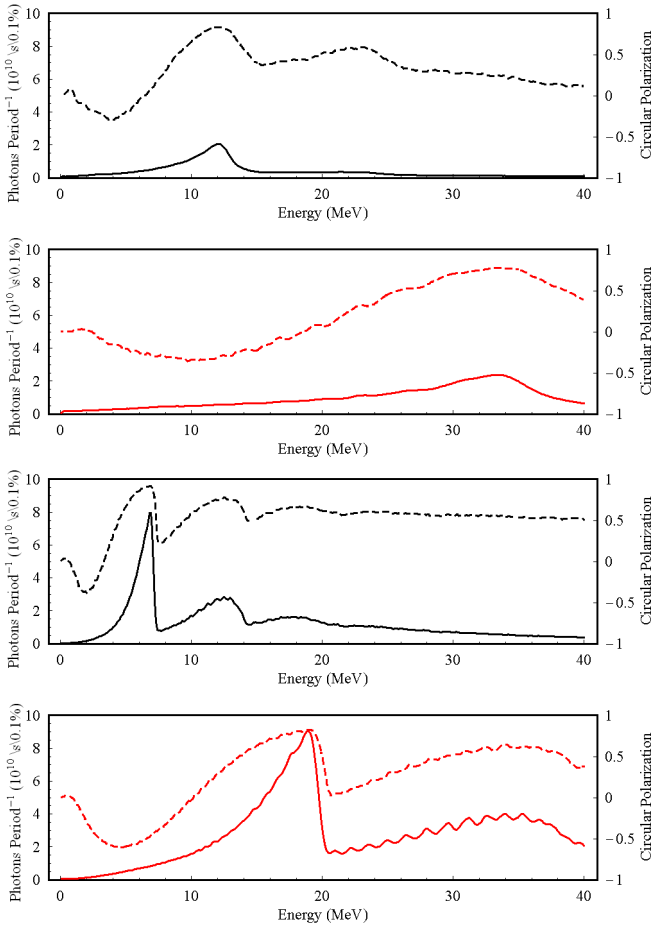

FIG. 17. (Color) Photon spectrum per period (solid) and circular polarization rate (dashed) from PM ring undulator (top) and SC undulator (bottom) for 150 GeV (black) and 250 GeV (red) energy electrons. Calculated using the measured magnetic flux density data.

TABLE III. ILC beam parameters used for flux and polarization calculation.

Parameter	Unit	Value
Beam energy	GeV	150, 250
Average current	μA	45
Natural emittance	nm rad	2×10^{-2}
Average β	m	25
Relative energy spread		0.0006

V. CONCLUSIONS AND FURTHER WORK

An investigation into possible helical undulator designs for the ILC positron source has been carried out. Based on the paper design study, two model undulators were constructed to assess the ease of fabrication and magnetic field quality. Both undulators produced a helical field distribution. The SC undulator performed to expectations but the PM ring one did not. For the PM ring undulator the field quality and strength were both less than expected.

This was due to the large number of components leading to possible assembly errors and demagnetization of the individual PM blocks during assembly. A tighter specification of magnet block errors would have ameliorated some of these problems, while the demagnetization effects would have been reduced if blocks with a higher coercivity had been manufactured, at the expense of a lower remanent field. The effects of magnet field errors could have been reduced by use of a block sorting algorithm, however this is not a practical solution for the full length ILC magnet as any sorting of the many hundreds of thousands of blocks required would be too time consuming. Exactly specifying the position and orientation of each block would also greatly increase the assembly time scale and complexity.

The reduction in field strength for the PM ring undulator means that a longer magnet would be required to achieve the required positron intensity for the ILC. For a K value of 0.4, 180 undulator photons are required to produce a single positron that takes part in collisions at the IP. For a K value of 1 only 140 photons are required to produce a similar positron. This is due to the different energy and angular spread of the photons. Therefore, if the PM ring undulator was to be used it would need to be approximately 30% longer than the SC undulator to give the same positron intensity at the IP. In general, as the degree of circular polarization is higher for the SC undulator , it would produce a higher positron polarization rate.

The trajectory of the electron beam through the SC undulator is significantly straighter than through the PM ring magnet. Although the values for the field integrals (Table II) are very small, it must be remembered that the undulators are both short, approximately 30 and 15 cm, respectively. Field correction along the length is not practical for either design and so the best field homogeneity must be achieved during manufacture. Simple trajectory correction will be done by using dipole correctors placed at the start and end of each module (typically every 4 m). A

TABLE IV. Peak flux and circular polarization values for SC and PM undulators.

Parameter	Unit	PM (150 GeV)	PM (250 GeV)	SC (150 GeV)	SC (250 GeV)
Peak flux energy	MeV	12.1	33.4	6.8	19.0
Peak flux	10^{10} Photons/period/s/0.1%	2.1	2.4	7.8	9.1
Peak CP energy	MeV	12.0	33.4	6.8	19.1
Peak CP rate		0.84	0.78	0.92	0.83

solution of this type is possible for the ILC undulator because of the very high energy beam and very small beam size. The SC undulator out-performs the PPM in terms of field homogeneity along the length. This will mean that the amount of dipole correction will be smaller and the possibility of deleterious trajectory walk-off of the electron beam is much smaller.

In terms of operational aspects, the SC undulator is also favored as the on-axis magnetic field can be controlled easily, allowing for a variable undulator K parameter if required. The SC undulator is also easy to switch off, whereas the PM ring magnet would have to have a gap control mechanism and support for the vacuum chamber in order to reduce the field on-axis to negligible levels. This is achievable but more involved than for the SC undulator. The ability to switch off the undulators will be beneficial during the commissioning of the ILC.

Another operational aspect that is difficult to quantify but could be important is the effect of radiation damage on the permanent magnets. The exact level of background radiation is not known. The undulator will be protected by a machine protection system and upstream collimators to stop gross damage but there will always be residual background radiation and beam halo particles to contend with. Radiation damage to PM undulators has been observed at the Advanced Photon Source [22]. The effects of radiation damage can be ameliorated by conditioning of the magnet, use of higher coercivity blocks, and operating the magnet at lower temperatures [23]. Operating the magnet at lower temperatures also increases the remanent field, however doing this would significantly increase the complexity of the engineering design in making sure the contraction of all the components was handled appropriately. It is not anticipated that the SC undulator would suffer from any significant radiation damage since the materials are already used in high radiation environments. This means that the SC undulator has a much lower risk of radiation damage.

To achieve the required vacuum level, the PM ring undulator would need significant development of NEG coating technology due to the very small aperture of the magnet. The SC undulator relies on cryopumping to achieve the required vacuum. Currently a round vessel a few meters in length with a $\sim$4 mm diameter has not been NEG coated. Coating a vessel of these dimensions would be a significant research activity in its own right. It is also unclear at the present time what the impedance effects of the NEG coating on the electron beam would be.

For all of these reasons (summarized below), the superconducting undulator has now been selected for the ILC positron source. In summary: (i) It performs better magnetically, resulting in a shorter overall length required to provide the same positron intensity. (ii) The field homogeneity is better, meaning that the amount of correction needed will be less and the trajectory wander of the electron beam will also be less. (iii) The K factor can be adjusted and the magnet is easy to switch off. (iv) The SC undulator will be less susceptible to any radiation damage. (v) There is a clear solution to provide the required vacuum needed for emittance preservation, requiring little further research and development. (vi) It has a better scope for further field enhancement since iron poles and an iron sleeve can be added relatively simply. (vii) The overall capital cost of the magnet is less (although the running cost would be higher).

Further work will look at the design of a SC undulator in more detail. The inclusion of iron poles and an iron sleeve will be considered to increase the on-axis flux. A reoptimization of the parameters, to account for the undulator being at the 150 GeV part of the linac, will also be completed. The conductor safety margin of 86% is also too high and the intention is to reduce this to 80%; although it should be noted that at no time during the experiment did the SC undulator quench. A full scale working prototype with cryostat will then be fabricated and tested with an electron beam.

ACKNOWLEDGMENTS

The authors gratefully thank members of the Magnets and Electrical Systems Group of the CERN Accelerator Technology Department for their help in the manufacture of the superconducting wire ribbon. The work is also supported by the Commission of the European Communities under the 6th Framework Programme Structuring the European Research Area, Contract No. RIDS-011899.

[1] ILC Baseline Configuration Document (BCD), http://www.linearcollider.org/wiki/.

[2] V. E. Balakin and A. A. Mikhailichenko, BINP 79-84, 1977.

[3] TESLA Technical Design report, DESY, 2001.

[4] G. A. Moortgat-Pick, T. Abe, G. Alexander, B. Ananthanarayan, A. A. Babich, V. Bharadwaj, D. Barber, A. Bartl, A. Brachmann, S. Chen, J. Clarke, J. E. Clendenin, J. Dainton, K. Desch, M. Diehl, B. Dobos, T. Dorland, H. Eberl, J. Ellis , K. Flöttmann, H. Fraas, F. Franco-Sollova, F. Franke, A. Freitas, J. Goodson, J. Gray, A. Han, S. Heinemeyer, S. Hesselbach, T. Hirose, K. Hohenwarter-Sodek, J. Kalinowski, T. Kernreiter, O. Kittel, S. Kraml, W. Majerotto, A. Martinez, H.-U. Martyn, W. Menges, A. A. Mikhailichenko, K. Mönig, K. Moffeit, S. Moretti, O. Nachtmann, F. Nagel, T. Nakanishi, U. Nauenberg, T. Omori, P. Osland, A. A. Pankov, N. Paver, R. Pitthan, R. Pöschl, W. Porod, J. Proulx, P. Richardson, S. Riemann, S. D. Rindani, T. G. Rizzo, P. Schüler, C. Schwanenberger, D. Scott, J. Sheppard, R. K. Singh, H. Spiesberger, A. Stahl, H. Steiner, A. Wagner, G. Weiglein, G. W. Wilson, M.

Woods, P. Zerwas, J. Zhang, and F. Zomer (POWER Collaboration), hep-ph/0507011.

[5] G. Alexander, P. Anthony, V. Bharadwaj, Y. K. Batygin, T. Behnke, S. Berridge, G. R. Bower, W. Bugg, R. Carr, E. Chudakov, J. E. Clendenin, F-J. Decker, Y. Efremenko, T. Fieguth, K. Flöttmann, M. Fukuda, V. Gharibyan, T. Handler, T. Hirose, R. H. Iverson, Y. Kamychkov, H. Kolanoski, T. Lohse, C. Lu, K. T. McDonald, N. Meyners, R. Michaels, A. A. Mikhailichenko, K. Mönig, G. Moortgat-Pick, M. Olson, T. Omori, D. Onoprienko, N. Pavel, R. Pitthan, M. Purohit, L. Rinolfi, K-P. Schüler, J. C. Sheppard, S. Spanier, A. Stahl, Z. M. Szalata, J. Turner, D. Walz, A. Weidemann, and J. Weisend (E166 Collaboration), SLAC-PROPOSAL-E166, 2002.

[6] K. T. Macdonald, J. Kovermann, A. Stahl, A. A. Mikhailichenko, D. Scott, G. A. Moortgat-Pick, V. Gharibyan, P. Pahl, R. Pöschl, P. Schüler, K. Laihem, S. Riemann, A. Schälicke, R. Dollan, H. Kolanoski, T. Lohse, T. Schweizer, Y. Batygin, V. Bharadwaj, G. Bower, F.-J. Decker, C. Hast, R. Iverson, J. C. Sheppard, Z. Szalata, D. Walz, A. Weidemann, G. Alexander, E. Reinherz-Aronis, S. Berridge, W. Bugg, and Y. Efrimenko (E166 Collaboration), in Proceedings of the 10th European Particle Accelerator Conference, Edinburgh, 2006.

[7] A. Hiraya, K. Yoshida, S. Yagi, M. Taniguchi, S.- Kimura, H. Hama, T. Takayama, and D. Amano, J. Synchrotron Radiat. **5**, 445 (1998).

[8] G. V. Rybalchenko, K. Shirasawa, M. Morita, N. V. Smolyakov, K. Goto, T. Matsui, and A. Hiraya, Nucl. Instrum. Methods Phys. Res., Sect. A **467–468**, 173 (2001).

[9] S. Sasaki, K. Miyata, and T. Takada, Jpn. J. Appl. Phys. **31**, L1794 (1992).

[10] The BESSY Soft X-ray Free Electron Laser Technical Design Report, BESSY, 2005.

[11] K. Halbach, Nucl. Instrum. Methods **169**, 1 (1980).

[12] M. S. Curtin, S. B. Segall, and P. Diament, Nucl. Instrum. Methods Phys. Res., Sect. A **237**, 395 (1985).

[13] P. Elleaume, O. Chubar, and J. Chavanne, in Proceedings of the 6th European Particle Accelerator Conference Stockholm, 1998, p. 3509.

[14] J. Pflüger (private communication).

[15] L. R. Elias and J. M. J. Madey, Rev. Sci. Instrum. **50**, 1335 (1979).

[16] T. A. Vsevolozhskaya, A. D. Chernyakin, A. A. Mikhailichenko, E. A. Perevedentsev, and G. I. Silvestrov, in Proceedings of the XIII International Conference in High Energy Accelerators, Novosibirsk, 1986.

[17] J. Rochford, E. Baynham, T. Bradshaw, A. Brummitt, S. Carr, Y. Ivanyushenkov, J. A. Clarke, O. B. Malyshev, D. J. Scott, I. R. Bailey, P. Cooke, J. B. Dainton, L. Malysheva, D. P. Barber, and G. A. Moortgat-Pick (Helical Collaboration), in Proceedings of the 10th European Particle Accelerator Conference, Edinburgh, 2006.

[18] Vector Fields Ltd., 24 Bankside, Kidlington, Oxford OX5 1JE, UK.

[19] VACUUMSCHMELZE GmbH, D 63412 Hanau, Germany.

[20] D. Bayham, R. Coombs, A. Ijspeert, and R. Perin, IEEE Trans. Magn. **30**, 1823 (1994).

[21] T. Tanaka and H. Kitamura, J. Synchrotron Radiat. **8**, 1221 (2001).

[22] S. Sasaki, I. B. Vasserman, C. R. Doose, E. R. Moog, and N. V. Mokhov, in Proceedings of the 2005 Particle Acclerator Conference, Knoxville, 2005.

[23] T. Bizen, X. Maréchel, T. Seike, H. Kitamura, T. Hara, T. Tanaka, Y. Asano, D. E. Kim, and H. S. Lee, in Proceedings of the 9th European Particle Acclerator Conference, Lucerne, 2004.